# Phase Transition and Rheological Behaviors of Concentrated Cellulose/Ionic Liquid Solutions

**Hongzan Song,[†,‡] Jun Zhang,[†] Yanhua Niu,[*,†] and Zhigang Wang[*,§]**

*CAS Key Laboratory of Engineering Plastics, Beijing National Laboratory for Molecular Sciences, Institute of Chemistry, Chinese Academy of Sciences, Beijing, 100190 P. R. China, Graduate School, Chinese Academy of Sciences, Beijing, 100049 P. R. China, and CAS Key Laboratory of Soft Matter Chemistry, Department of Polymer Science and Engineering, Hefei National Laboratory for Physical Sciences at the Microscale, University of Science and Technology of China, Hefei, Anhui Province 230026 P. R. China*

*Received: February 14, 2010; Revised Manuscript Received: March 30, 2010*

The phase transition and rheological behaviors of concentrated solutions of microcrystalline cellulose (MCC) in an ionic liquid of 1-allyl-3-methylimidazolium chloride (AMIMCl) have been investigated. Polarized optical microscopy (POM) measurements indicate that the two critical cellulose concentrations for the appearance of biphase and fully anisotropic phase for MCC/AMIMCl solutions are 9 and 16 wt%, respectively. POM and differential scanning calorimetry (DSC) measurements coherently indicate that the clearing temperature, $T_c$ increases with increasing cellulose concentration. Oscillatory shear measurements show that the crossover frequency first moves to lower values and then moves back to higher values with increasing cellulose concentration, which indicates that most cellulose chains are aligned or oriented to reduce chain entanglements when the cellulose concentration is above 14 wt%. From the steady shear measurements, it is surprising to find that the viscosity versus shear rate curves exhibit four flow regions including two plateaus and two shear-thinning regions when the cellulose concentration exceeds 9 wt%. The influences of cellulose concentration and temperature on the first normal stress differences ($N_1$) are analyzed according to the Larson theory. The peak of $N_1$ always appears at the intermediate part of the first shear-thinning region, and the following minimum of $N_1$ appears at the onset of the second shear-thinning region. The viscosity versus shear rate curves only exhibit two flow regions when temperature is above the respective $T_c$; meanwhile, negative $N_1$ values disappear and $N_1$ increases monotonically. The above results suggest that melting of the liquid crystal domains at high temperature results in the disappearance of the second plateau for the viscosity versus shear rate curves.

## 1. Introduction

Cellulose, as the most plentiful and renewable resource in the world, is not soluble, however, in water or conventional organic solvents due to its strong intermolecular hydrogen bonding.[1−6] Ionic liquids (ILs), as newly developed solvents, exhibit a powerful capacity to dissolve cellulose.[7−9] Recently, studies on the application of ILs in cellulose chemistry have attracted much attention, including the preparation of some new functional cellulose materials by using ILs,[10,11] syntheses of more kinds of cellulose derivatives in ILs,[12,13] and depolymerization of cellulose using solid catalysts in ILs.[14] Nowadays, ILs used for manufacturing-regenerated cellulose fibers are arousing considerable commercial interest because of their superior dissolving capacity, environmentally friendly properties, easy recycling, and good recoverability.[15,16] However, mechanical properties for the most frequently regenerated cellulose fibers spun from ILs are unsuitable compared with those of viscous and Lyocell-type fibers, which precludes the industrial application of cellulose fibers produced by using ILs.[15] It is well-known that fibers produced from liquid crystal polymers (LCPs) have outstanding mechanical properties due to their intrinsic, highly oriented, rigid backbones and strong intermolecular secondary bonds.[17,18] The previous investigations indicate that natural cellulose and many of its derivatives are, in principle, capable of forming cholesteric or twisted nematic phases in suitable solvents.[19−21] More specifically, Rogers et al.[22] and Zhang et al.[23] have reported that cellulose/ionic liquid solutions appear optically anisotropic when cellulose is dissolved at high concentrations. Therefore, the formation of liquid crystalline phases in the cellulose/ionic liquid solutions makes possible the generation of high performance cellulose materials.

It has long been recognized that the spinning process and fiber properties of liquid crystalline polymers (LCPs) are directly related to their rheological properties and the applied shear field.[24−28] The main focus of rheological studies on LCPs is the remarkable change in the first normal stress differences ($N_1$) with increasing shear rate during steady shear flow.[29−33] For thermotropic LCPs, only positive $N_1$ values could be observed,[31,34] while for lyotropic LCP solutions, previous investigations[24,29,35] revealed that $N_1$ as a function of shear rate could be divided into three regions: positive, negative, and the second positive regions. Meanwhile, several theoretical attempts have been made to explain the origin of such an unusual experimental observation.[36,37] Marrucci and Maffettone[38,39] considered that the occurrence of negative $N_1$ was associated with flow transition between director tumbling and flow-aligning behavior. Larson[40] concluded that the negative $N_1$ occurred in the "wagging" regime representing the transition from the tumbling to the nontumbling

* Corresponding authors. Tel/Fax: 011-86-10-62558172. E-mail: (Y.-H.N.) yhniu@iccas.ac.cn; (Z.-G.W.) zgwang2@ustc.edu.cn.
† Institute of Chemistry, Chinese Academy of Sciences.
‡ Graduate School, Chinese Academy of Sciences.
§ University of Science and Technology of China.

10.1021/jp1013863 
Published on Web 04/20/2010

flow (flow-aligning) regime. Obviously, rheological properties of traditional LCPs have been extensively investigated. However, for the newly developed cellulose/ionic liquid solutions, less work about their liquid crystalline phase transitions and related rheological behaviors has been reported up to now. Further exploration on this topic is of great importance from both theoretical and industrial considerations.

In our previous work, the structure and dynamics of the ionic liquid of AMIMCl were studied by using dynamic light scattering (DLS),[5] and then the rheological properties of cellulose/AMIMCl solutions with concentrations ranging from dilute to semidilute regimes under both oscillatory and steady shear modes were further studied.[41] For concentrated cellulose/AMIMCl solutions, however, situations might be quite different due to the possible phase transition behaviors. In this study, the phase transition and rheological behaviors of concentrated solutions of microcrystalline cellulose (MCC) dissolved in the ionic liquid of 1-allyl-3-methylimidazolium chloride (AMIMCl) were investigated by using polarized optical microscopy (POM), differential scanning calorimetry (DSC), and rheometry. Studies were conducted to characterize the influences of cellulose concentration and temperature on the phase transition and rheological behaviors of the MCC/AMIMCl solutions. The unique rheological properties including the variations of viscosity $\eta$ and $N_1$ under steady shear at different temperatures were observed.

## 2. Experimental Section

**2.1. Materials and Sample Preparation.** The ionic liquid of 1-allyl-3-methylimidazolium chloride (AMIMCl) as a good solvent for cellulose was synthesized according to the procedure described in the literature.[23] Purification of AMIMCl was carried out on the basis of our previous work.[5] The chemical identity and purity of the AMIMCl were also confirmed by $^1$H-nuclear magnetic resonance (NMR) measurement. The water content of AMIMCl measured by Karl−Fischer titration was 0.12 wt%. Microcrystalline cellulose (MCC), Vivapur 101, used in this study was purchased from the Sen-Jun Chemical Agents Accessories Co., Ltd., Shanghai, China. The viscosity-average degree of polymerization (DP) of MCC in cupriethylenediamine hydroxide solution is about 200 as measured by using an Ubbelodh viscometer.

MCC/AMIMCl solutions with high concentrations ranging from 7 to 19 wt% were prepared. For each solution preparation, a certain amount of cellulose was first added into a 25 mL conical flask containing AMIMCl. The flask was quickly sealed to avoid water adsorption. The suspension was then gently stirred at 90 °C for 4 h to obtain a homogeneous solution. Note that when the solutions with very high cellulose concentrations were prepared, it was necessary to stir the solutions for a long time and remove air bubbles by reducing the pressure. The water content in each solution measured by the Karl−Fischer titration was about 0.15 wt%. Before further measurements, the solutions were sealed and stored in desiccators containing $P_2O_5$.

**2.2. Characterization Methods.** ***2.2.1. Rheological Measurements.*** Rheological properties of the MCC/AMIMCl solutions under both oscillatory and steady shear modes were measured by using a TA AR2000 stress-controlled rheometer with a 25 or 40 mm parallel-plate geometry. The chosen gap was about 600 $\mu$m for all the measurements. Steady shear measurements and dynamic frequency sweep measurements were carried out within the shear rate range of 0.01−100 $s^{-1}$ and frequency range of 0.1−100 rad/s, respectively. The selected strain of 15% during the frequency sweeps fell well into the linear viscoelastic regime. The experimental temperature was mainly set at 25 °C, which was higher than the melting point of AMIMCl. All measurements were conducted under a nitrogen atmosphere.

***2.2.2. Optical Microscope Observations.*** The MCC/AMIMCl solutions with different concentrations were pressed between two cover glasses with a thickness of about 100 $\mu$m. A homemade hot stage with temperature fluctuations within ±0.1 °C was applied to control the sample temperatures. Optical micrographs were then taken by using the BX51 Olympus polarized optical microscope equipped with a Pixera Penguin 150CL CCD camera. A 530 nm sensitive tint plate (1$\lambda$, U-TP530, Olympus) was used as a test plate compensator, which resulted in a magenta background for the micrographs. All the observations were conducted under a nitrogen atmosphere.

***2.2.3. Phase Transition Behaviors by Differential Scanning Calorimetry (DSC).*** The phase transition behaviors of the MCC/AMIMCl solutions were also traced by using a TA Q200 DSC instrument with a sample weight of about 5.0 mg. The samples were heated from −50 to 150 °C at a heating rate of 10 °C/min under a nitrogen atmosphere.

## 3. Results and Discussion

**3.1. Lyotropic Liquid Crystalline Behaviors of Cellulose Solutions.** Cellulose solutions are, in principle, capable of forming cholesteric or twisted nematic phases in suitable solvents over critical concentrations.[19−21] In general, the solution forming lyotropic liquid crystals has two critical concentrations of $C_1$ and $C_2$. Below $C_1$ the solution is isotropic, above $C_2$ the solution is fully anisotropic, and between $C_1$ and $C_2$ the solution shows a biphase (a mixture of isotropic and anisotropic phases). Polarized optical microscopy (POM) was first used to determine the critical concentrations for the MCC/AMIMCl solutions to form lyotropic liquid crystals.[26,42] Figure 1 shows the polarized optical micrographs of the MCC/AMIMCl solutions at 25 °C. Note the micrographs are taken with the sensitive tint plate insertion, in order to clearly show the phase transitions. The visible color changes and the related structure transitions are clearly distinguished. For the 7 wt% concentration solution, no anisotropic texture is observed, indicating it is an isotropic solution. (We note that without the sensitive tint plate insertion the isotropic phase appears black. The micrograph is not shown.) With increasing cellulose concentration up to about 9 wt%, weak fingerprint-like textures with slight yellow and purple interface colors appear. The micrograph taken without using the sensitive tint plate is shown in the inset, from which the fingerprint-like textures are seen. Such a pattern indicates the initial formation of a cholesteric phase. Stronger fingerprint-like textures are observed for the 11 wt% concentration solution. When the cellulose concentration is raised to 14 wt%, the lyotropic liquid crystal solution appears as a nonaligned cholesteric phase[43] and shows planar textures.[44] The reason for the appearance of the nonaligned cholesteric phase rather than the regular textures may lie in the high viscosity of the MCC/AMIMCl solutions; such high viscosity prevents the migration or aggregation of the liquid crystalline phase into more organized domains. At the high concentration of 16 wt%, a blue color appears and a strong optical planar texture forms, which is an obvious signature of the fully anisotropic phase. Very strong optical planar textures and intense colors are observed for the 18 wt% concentration solution. Thus, the optical microscope observations indicate that the two critical concentrations $C_1$ and $C_2$ for the MCC/AMIMCl solutions to form lyotropic liquid crystals are 9 and 16 wt%, respectively.

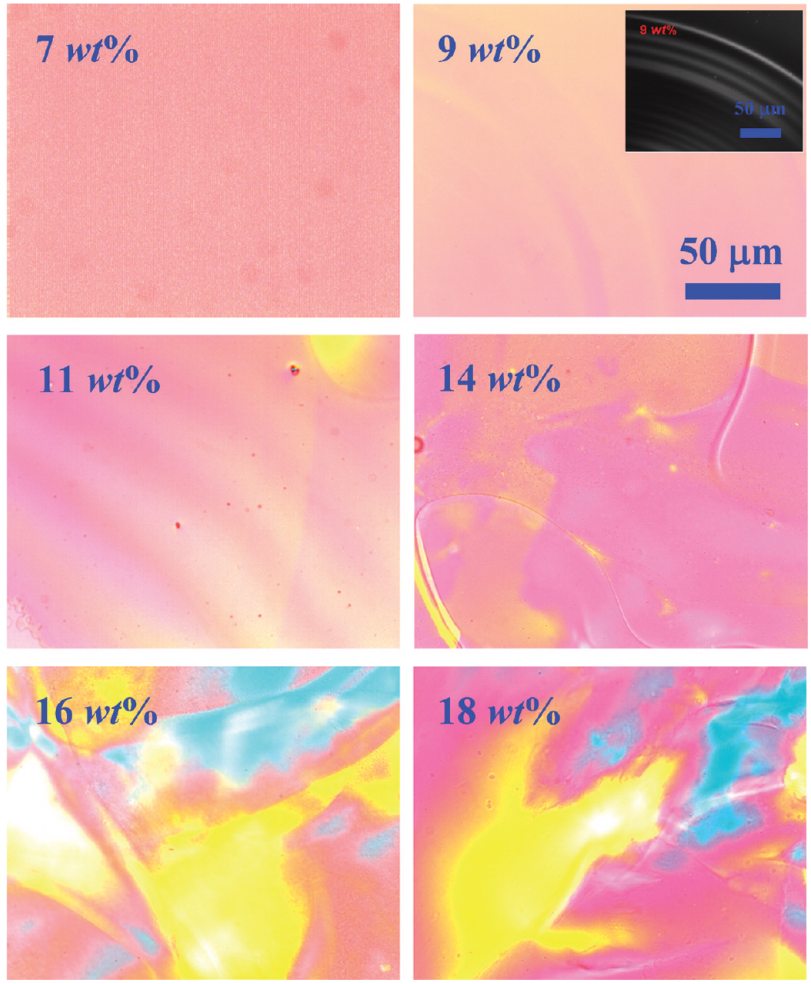


**Figure 1.** Polarized optical micrographs of the MCC/AMIMCl solutions with different concentrations at 25 °C with the sensitive tint plate insertion. Inset: the micrograph taken without the sensitive tint plate insertion for the 9 wt% concentration solution.

To further investigate the temperature dependence of lyotropic liquid crystal formation in the MCC/AMIMCl solutions, polarized optical microscope observations for temperatures ranging from 25 to 80 °C were conducted. Figure 2 shows the typical optical micrographs for the 16 wt% MCC/AMIMCl solution at different temperatures. With increasing temperature, the blue parts of the texture fade first and disappear completely at 75 °C, while the yellow parts fade gradually and disappear completely at 80 °C. The completely featureless optical micrograph at 80 °C represents the isotropic phase for the 16 wt% MCC/AMIMCl solution. The temperature of 80 °C is termed as the clearing temperature ($T_c$) for the 16 wt% MCC/AMIMCl solution. The change of $T_c$ values with concentration for all the solutions is shown in Figure 3. Once the anisotropic texture disappears upon heating, its recovery during cooling is slow, taking several days.

Figure 4 shows the DSC heat flow curves during heating for the MCC/AMIMCl solutions with different concentrations. As can be seen, an endothermic peak corresponding to the melting of the cholesteric liquid crystal phase appears when the cellulose concentration exceeds 9 wt%. With increasing cellulose concentration, the peak value shifts to higher temperature and meanwhile the peak area becomes larger, which is consistent with the optical microscope observations and can be explained by the increased anisotropic phase content and ordering degree in the MCC/AMIMCl solutions. The peak value is termed as the clearing temperature ($T_c$) of the solution by the DSC method. The change of $T_c$ values with concentration as determined by the DSC method is also shown in Figure 3.

Figure 3 actually represents a phase diagram with temperature on the vertical scale and concentration on the horizontal scale for the MCC/AMIMCl solutions. The data points determined from the DSC measurements show a good agreement with that from the POM measurements, which indicates the accuracy of the phase diagram. It is seen that $T_c$ obviously increases with increasing cellulose concentration, which is due to the increased ordering degree of the anisotropic phase. Through careful examination, we find that the slope for the cellulose concentration increasing from 9 to 11 wt% is larger than that from 14 to 18 wt%, which is attributed to the formation of nonaligned cholesteric phase for the high cellulose concentration solutions. Note that the 7 wt% MCC/AMIMCl solution always shows isotropic phase at room temperature and the other higher concentration solutions show obviously anisotropic or specifically the cholesteric phase at room temperature. Therefore, the following discussion on rheological measurements will be based on this phase diagram.

**3.2. Dynamic Viscoelastic Behaviors.** The changes of storage ($G'$) and loss ($G''$) moduli as a function of angular frequency for the MCC/AMIMCl solutions with different concentrations at 25 °C are shown in Figure 5. For the solutions with MCC concentration below 9 wt%, $G'$ is always smaller than $G''$ and no crossover is found within the detected frequency range. However, the crossover may locate at higher frequencies because even the lowest concentration of 7 wt% in this study is far beyond the cellulose entanglement concentration of about 1.5 wt% according to our previous study.[41] As the cellulose

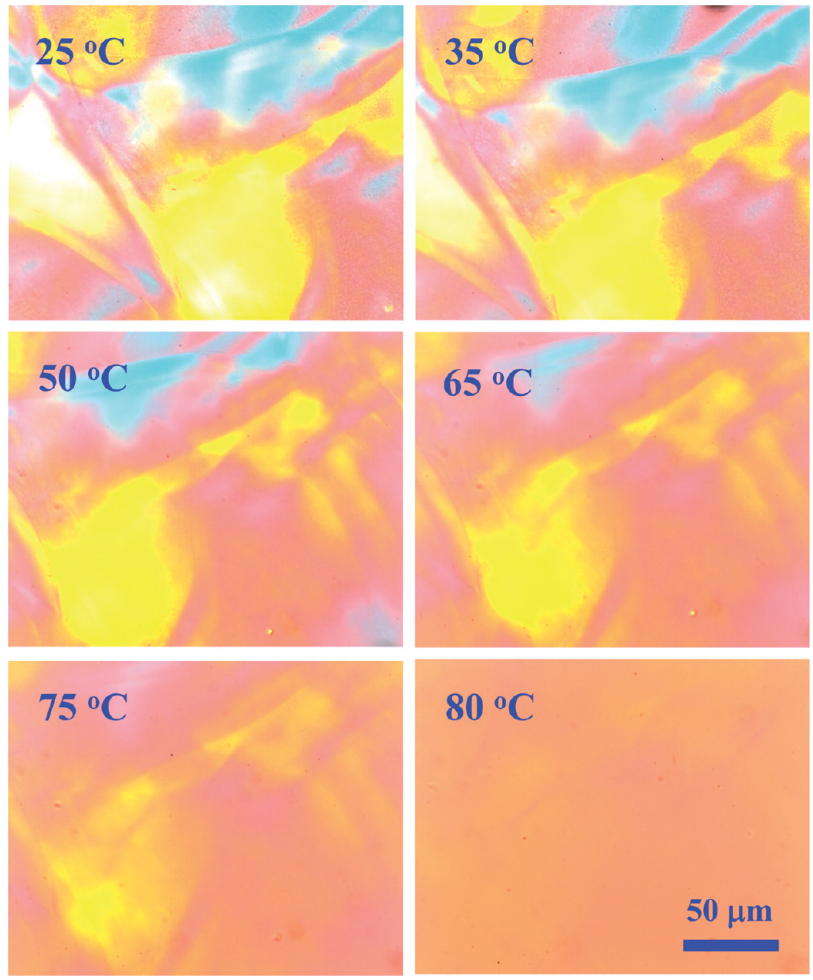


**Figure 2.** Polarized optical micrographs for the 16 wt% MCC/AMIMCl solution at different temperatures with the sensitive tint plate insertion.

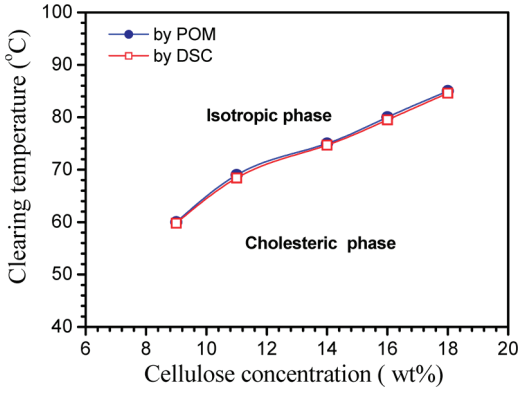


**Figure 3.** Phase diagram of the MCC/AMIMCl solutions determined from the POM and DSC measurements.

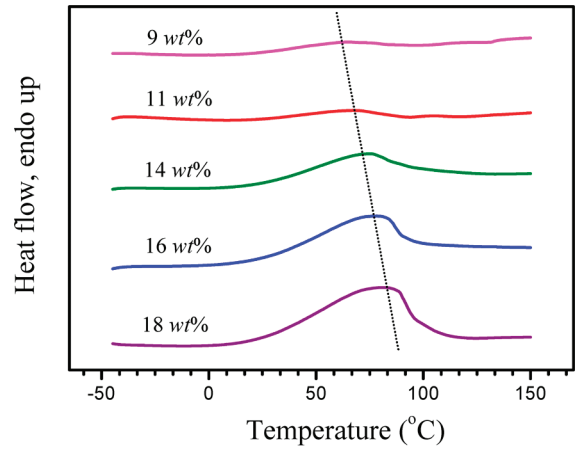


**Figure 4.** DSC heat flow curves during heating for the MCC/AMIMCl solutions with different concentrations.

concentration increases from 11 to 14 wt%, $G' < G''$ only occurs at low frequencies and a crossover appears at a higher frequency. Within the concentration from 7 to 14 wt%, the crossover frequency evidently moves to lower values with increasing cellulose concentration, which indicates a significant slowing of the cellulose chain relaxation. Interestingly, when the cellulose concentration continually increases, the crossover frequency moves back to higher values and even disappears for the solution with concentration of 18 wt%. There are two competitive processes to influence the cellulose chain relaxation: one is the substantial chain entanglement, and the other is the phase transition-induced chain alignment. When the cellulose concentration is below 14 wt%, the chain entanglement predominates, with entanglement density increasing with increasing cellulose concentration and therefore slows the cellulose chain relaxation. However, when the cellulose concentration is above a critical concentration, the content of the anisotropic liquid crystal phase exceeds that of the isotropic phase, for which most cellulose chain segments can be aligned to lower the flow energy and further reduce chain entanglements.[45] When the cellulose chain segments have less rotational hindrance, cellulose chain relaxation can become faster.

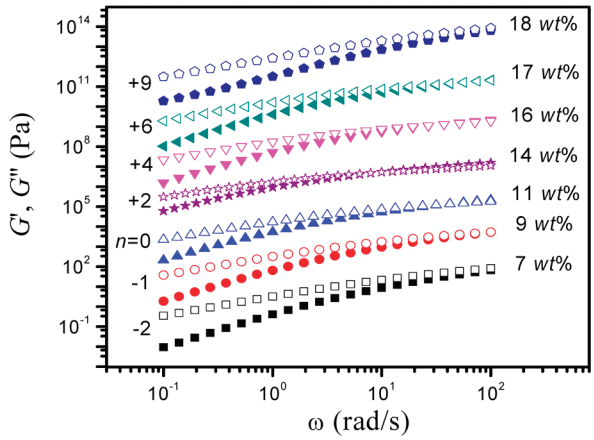


**Figure 5.** Changes of storage ($G'$, solid symbol) and loss ($G''$, open symbol) moduli as a function of frequency for the MCC/AMIMCl solutions with different concentrations at 25 °C. The data are shifted along the vertical axis by multiplying $10^n$ with corresponding $n$ values of −2, −1, 0, 2, 4, 6 and 9, respectively, to prevent data overlap.

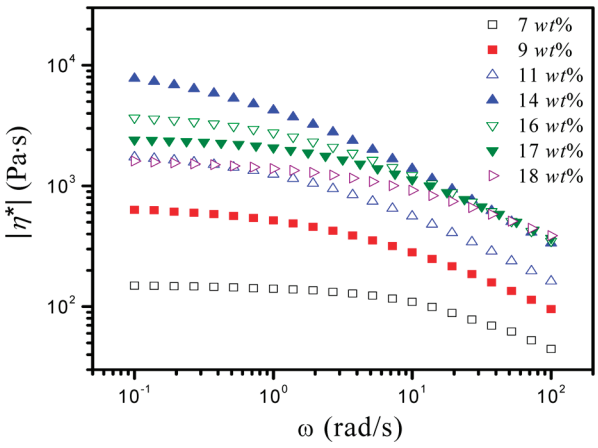


**Figure 6.** Change of complex viscosity as a function of frequency for the MCC/AMIMCl solutions with different concentrations at 25 °C.

Figure 6 shows the changes of complex viscosity, $|\eta^*|$, as a function of angular frequency for the MCC/AMIMCl solutions with different concentrations at 25 °C. The most prominent feature is that the $|\eta^*|$ values at low frequencies first increase (from 7 to 14 wt%) and then decrease (from 14 to 18 wt%) with increasing concentration. The decrease of $|\eta^*|$ values indicates the formation and enhancement of the aligned or oriented cellulose chains. Another easily observable phenomenon for the MCC/AMIMCl solutions is that the $|\eta^*|$ values at high frequencies tend to converge to a common curve when the cellulose concentration exceeds 11 wt%.

**3.3. Steady Shear Behaviors.** Steady shear measurements were made over a range of shear rate for the MCC/AMIMCl solutions with different concentrations at 25 °C, and the changes of viscosity as a function of shear rate are shown in Figure 7. For the solution with the low cellulose concentration, i.e., 7 wt%, a broad Newtonian plateau appears at low shear rates and one shear-thinning region appears at high shear rates, which is similar to that of conventional isotropic polymeric fluids.[46,47] With increasing cellulose concentration, the Newtonian plateau evidently becomes narrower and the shear-thinning behavior becomes more complex. When the cellulose concentration exceeds 9 wt%, four flow regions are observed, which are the first Newtonian plateau and the shear-thinning region at low shear rates, and the second plateau or step and the final shear-thinning region at high shear rates. This observation is different

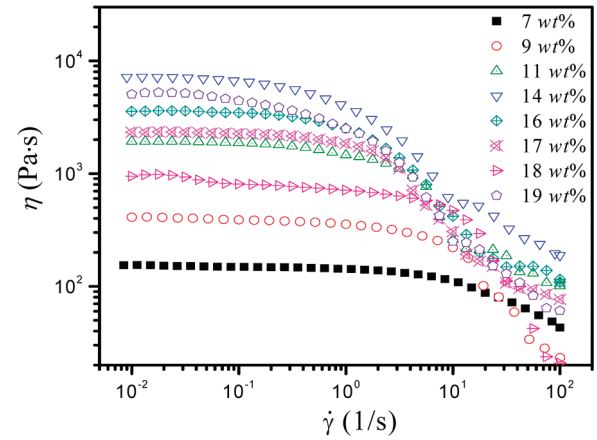


**Figure 7.** Steady shear flow curves for the MCC/AMIMCl solutions with different concentrations at 25 °C.

from others,[32,35,48−51] in which the well-known three-region flow curve was observed including two shear-thinning regions at low and high shear rates (flow regions I and III, respectively) and a plateau region at intermediate shear rates (flow region II). The appearance of the first Newtonian plateau at low shear rates in our study has been predicted by the modified Doi theory[36] and proved in several experimental observations.[29,30] According to the modified Doi theory, the plateau region at low shear rates can be attributed to interdomain interactions. It has been reported that the formed cholesteric liquid crystal phase for the MCC/AMIMCl solutions above a critical concentration can convert into a nematic phase under shear.[29,52,53] Therefore, it is thought that a transition from the cholesteric to nematic liquid crystal phases may occur at low shear rates, and then the nematic cellulose solutions exhibit a typical three-region flow curve including shear-thinning at low and high shear rates and about constant viscosity values at intermediate shear rates. The phase transition from cholesteric to nematic phases can induce a viscosity decrease due to the higher ordering degree of the latter. For the low concentration solutions, the cholesteric phase content is so small that the viscosity decrease induced by the phase transition cannot be obviously observed. Nevertheless the flow curve for the 18 wt% MCC/AMIMCl solution shows an inflection point at a shear rate of 0.03 $s^{-1}$ with a gradual viscosity decrease, and the subsequent part of the flow curve shows a typical three-region flow. This result further confirms our considerations and indicates that the shear-induced cholesteric to nematic transition is not an instantaneous but rather a durative process.[29] For the solution with a concentration of 19 wt%, such viscosity inflection induced by phase transition is not so evident, but a slight decrease is still observable, which in our opinion is due to the compact packing of cellulose chains at high concentration, so the chain segment rotation is somewhat hindered and hence the phase transition becomes difficult. Besides, the high viscosity of the 19 wt% MCC/AMIMCl solution at low shear rates also ascribes to the compact packing of the cholesteric phase.

Figure 8 illustrates the change of the zero-shear viscosity, $\eta_0$, with cellulose concentration. The zero-shear viscosity can be obtained by fitting the viscosity curve through the Cross model. With increasing cellulose concentration, $\eta_0$ shows a slight increase below a concentration of 11 wt%, a steep increase up to the maximum value at a concentration of 14 wt%, a sharp drop to the minimum value at a concentration of 18 wt%, and a steep increase again. The first dramatic increase and then a following sharp decrease for $\eta_0$ with increasing concentration is a typical behavior for lyotropic liquid crystal materials.[26,29]

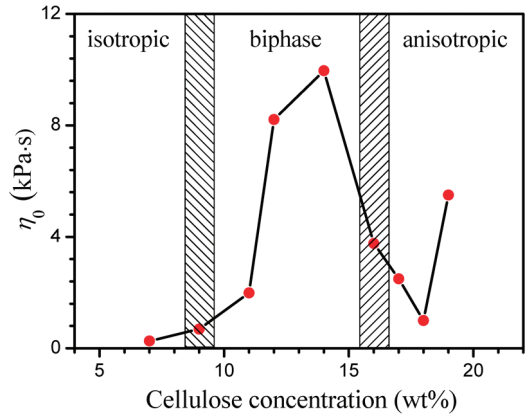


**Figure 8.** Change of the zero-shear viscosity, $\eta_0$, with cellulose concentration for the MCC/AMIMCl solutions.

Combined with the polarized optical microscope observations as shown in Figure 1, the viscosity−concentration curve for the MCC/AMIMCl solutions as shown in Figure 8 can be separated into three concentration regions corresponding to the isotropic, biphase, and anisotropic phases, respectively. The shadow areas represent the phase transition zones. This observation is quite similar to many others for different lyotropic liquid crystal solutions.[27,54,55] In addition, the biphase-related structure in the solution is mainly responsible for its relatively high viscosity.

**3.4. The Cox−Merz Rule.** According to the Cox−Merz rule, the complex viscosity, $|\eta^*|$, is equal to the steady shear viscosity, $\eta$, when the angular frequency and shear rate approximately approach zero. Figure 9a shows that the Cox−Merz rule works well for the isotropic cellulose solution (7 wt%) because $|\eta^*|$ and $\eta$ superpose with each other within the whole angular frequency or shear rate ranges, which indicates that the steady shear can hardly influence the chain entanglements due to strong hydrogen bond interactions between cellulose and the ionic liquid. However, Figure 9b shows that $\eta$ deviates obviously from $|\eta^*|$ at high shear rates for the biphase cellulose solution (14 wt%), which is considered to be caused by shear-induced slippage and alignment of cellulose chains in the liquid crystal phase under large deformations.[35,55] This is also a common phenomenon for liquid crystalline polymers (LCPs). Furthermore, Figure 9c shows that $|\eta^*|$ values are always higher than $\eta$ values over the entire angular frequency and shear rate ranges for the fully anisotropic cellulose solution (18 wt%). Kulicke et al.[55] and Oertel et al.[26] concluded that the deviations from the Cox−Merz rule could be explained by changes of intra- and intermolecular hydrogen bonds. Recently, the experimental studies by Zhang et al.,[23] who speculated the dissolution mechanism of cellulose in AMIMCl, and by Wang et al.,[56] who captured the portrait of isolated individual cellulose molecules in AMIMCl, indicated the existence of strong interactions between cellulose and the ionic liquid. So we suggest herein that the deviations from the Cox−Merz rule occurring in the concentrated MCC/AMIMCl solutions are due to the destruction of strong intra- and intermolecular hydrogen bonds between cellulose and the ionic liquid under shear deformation.

Figure 10 shows the shear rate dependences of the first normal stress differences ($N_1$) for the MCC/AMIMCl solutions with different concentrations at 25 °C. First of all, $N_1$ values are positive over the entire shear rate ranges for all the solutions, which is similar to the results of Kim and Han.[31,34] Second, for the isotropic cellulose solution (7 wt%), $N_1$ increases monotonically with increasing shear rate. However, for each biphase

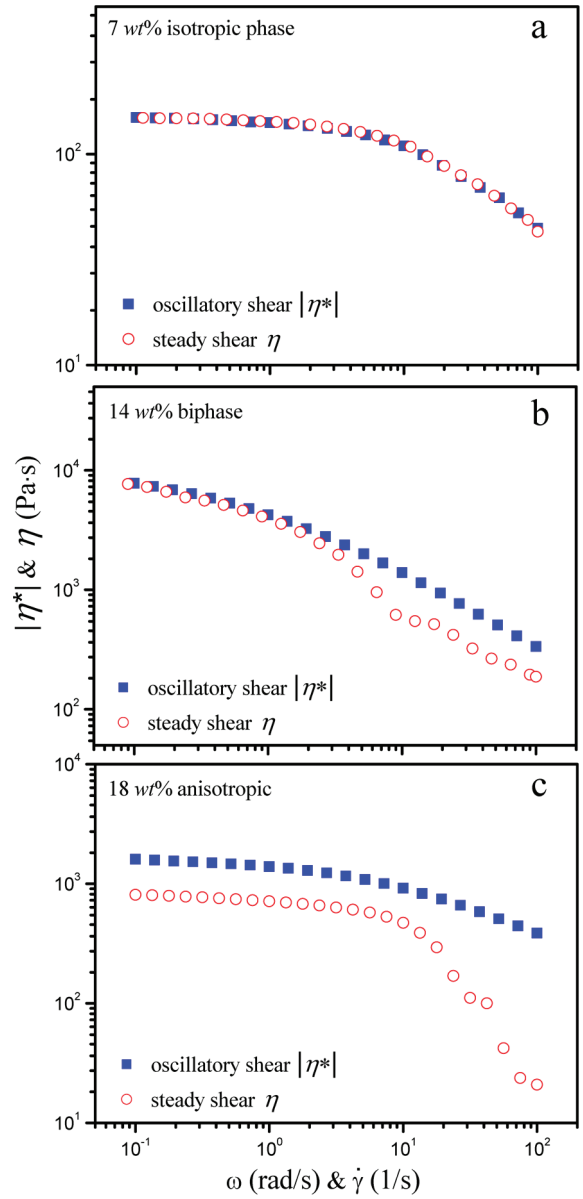


**Figure 9.** The Cox−Merz rule for the MCC/AMIMCl solutions with different concentrations of (a) 7 wt%, (b) 14 wt%, and (c) 18 wt% at 25 °C.

cellulose solution (9 to 14 wt%), the $N_1-\dot{\gamma}$ curve deviates from monotonic increase and a narrow plateau in the intermediate shear rate range appears. Furthermore, for the fully anisotropic cellulose solutions (16 to 18 wt%), the $N_1-\dot{\gamma}$ curves are somehow similar to that in other reports;[29,35,57] however, the negative $N_1$ regions do not appear. Instead, the relatively *positive* minima in $N_1$ are retained. According to the Larson theory,[40,58] the strong tumbling and the negative $N_1$ region will occur in cases where the Deborah number (De) $\ll 1$ at low shear rates (De $\equiv \tau\dot{\gamma}$, where $\tau$ is the molecular relaxation time and $\dot{\gamma}$ is shear rate) and where the molecular elasticity is negligible. While the molecular elasticity must be considered when De $\geq$ 1, the weak tumbling regime will occur when De $\approx$ 1, and the tumbling regime and the minimum in $N_1$ may disappear at a high De value. Moreover, Larson[56] concluded that the minimum in $N_1$, whether positive or negative, sufficed to reveal the existence of tumbling. On the basis of the dynamic frequency sweep measurements, $\tau$ can be determined and the De values at 25 °C in this study are close to 1 at low shear rates, which may lead to weak tumbling. Furthermore, the molecular

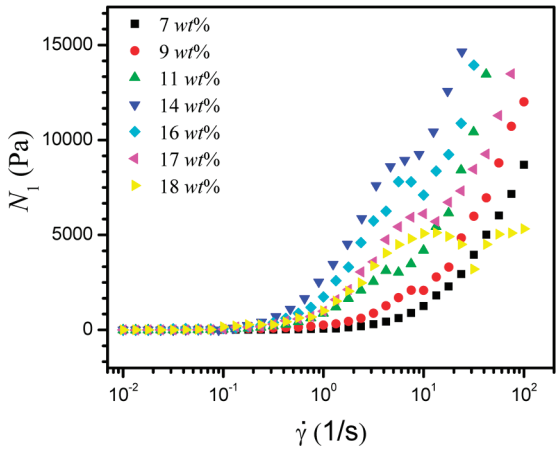


**Figure 10.** Changes of the first normal stress differences, $N_1$, as a function of shear rate for the MCC/AMIMCl solutions with different concentrations at 25 °C.

relaxation time and De decrease with increasing concentration from 16 to 18 wt% when the shear rate and temperature are held constant, which may lead to strong tumbling and cause the $N_1$ values to decrease and tend to approach negative values.

In general, lower temperature corresponds to higher De largely because of increased relaxation time. Therefore, we predict that an increase of temperature can lead to an appearance of negative $N_1$ because of strong tumbling. Figure 11 compares the shear rate dependences of $N_1$ and $\eta$ for the 14 and 18 wt% MCC/AMIMCl solutions at different temperatures. As shown in Figure 11a, for the 14 wt% solution at a low temperature of 30 °C, $N_1$ gradually increases until a plateau appears at a shear rate of about $\dot{\gamma} = 6.3\ s^{-1}$, and then $N_1$ sharply increases. At a temperature of 50 °C, an obvious peak appears at $\dot{\gamma} = 6.3\ s^{-1}$, and a minimum of $N_1$ appears at $\dot{\gamma} = 10.6\ s^{-1}$. The situation at higher temperatures is rather different, that is, the minimum of $N_1$ is too tiny to observe at 70 °C and even disappears at 75 °C. Moreover, the shear rate at which the characteristic plateau or minimum appears shifts to a higher value with increasing temperature. This is because the increase of temperature is expected to reduce the liquid crystal ordering parameter by increasing polymer chain flexibility as the clearing temperature is approached.[32] Furthermore, Baek et al.[50] and Aden et al.[59] have concluded that the strong tumbling at high temperatures may occur for lyotropic liquid crystal solutions with short persistence lengths. Therefore, alignments of cellulose chains along the flow direction occur at the high shear rates. The disappearance of $N_1$ minimum at 75 °C is an obvious indication of the isotropic solution. Interestingly, the peak and minimum of $N_1$ are more obvious for the 18 wt% cellulose solution, and the predicted negative $N_1$ values eventually appear at a temperature of 70 °C as shown in Figure 11c. Moreover, a temperature of 85 °C at which the minimum of $N_1$ disappears for the 18 wt% cellulose solution is much higher than that of 75 °C for the 14 wt% cellulose solution.

Comparing the variations of $N_1$ and $\eta$ at the same conditions, we found that the peak of $N_1$ always appears at the intermediate part of the first shear-thinning region and the following minimum of $N_1$ corresponds to onset of the second shear-thinning region. On the other hand, all the $\eta-\dot{\gamma}$ curves exhibit four flow regions over the entire shear rate range besides the initial decrease at low shear rates when the temperatures are below the respective $T_c$ (see Figure 11b,d) whereas the $\eta-\dot{\gamma}$ curves only exhibit two flow regions when the temperatures are above $T_c$. Meanwhile, the negative $N_1$ values disappear and

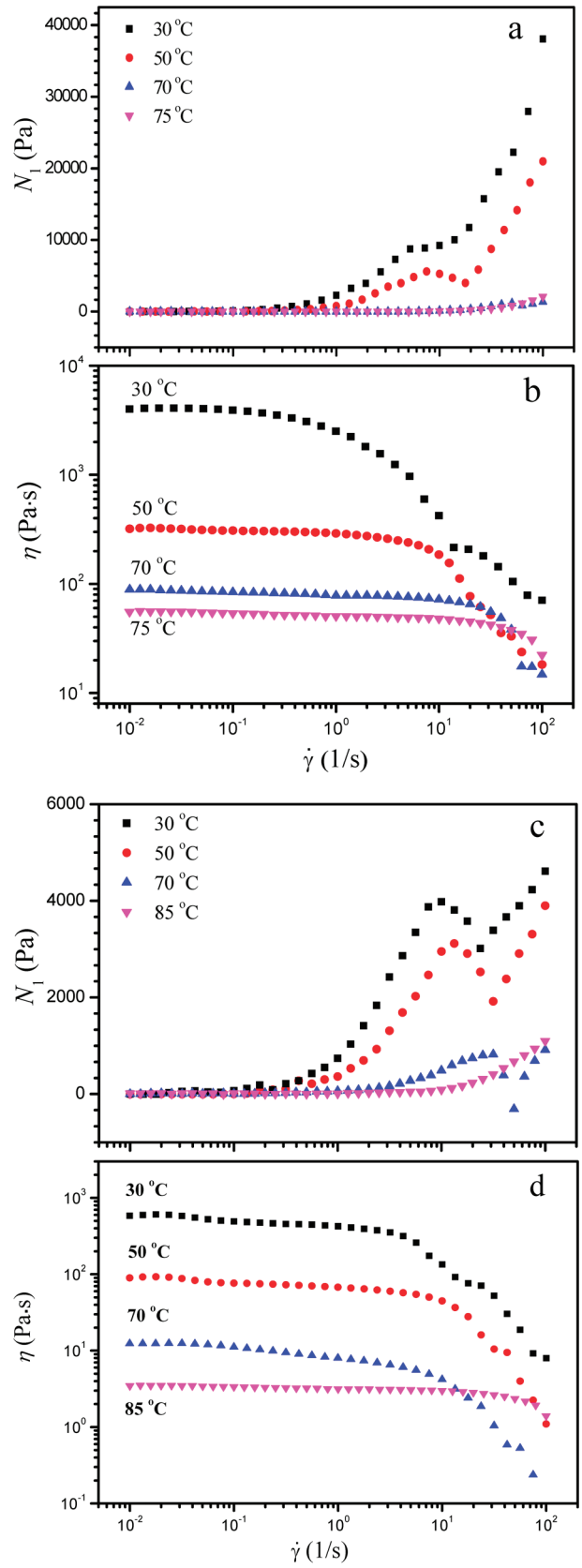


**Figure 11.** Shear rate dependences of the first normal stress differences $N_1$ (a, c) and viscosity $\eta$ (b, d) during steady shear flows for the 14 wt% (a, b) and 18 wt% (c, d) MCC/AMIMCl solutions at different temperatures.

$N_1$ increases monotonically, indicating melting of the liquid crystal domains at the high temperatures.

## 4. Conclusions

In this study the phase transition and rheological behaviors of the concentrated MCC/AMIMCl solutions were investigated. Two critical cellulose concentrations corresponding to the transitions from isotropic to biphase and biphase to anisotropic phases for the MCC/AMIMCl solutions were 9 and 16 wt%, respectively. The clearing temperature ($T_c$) increased with increasing cellulose concentration.

The results from dynamic frequency sweep measurements indicated that most cellulose chains were aligned and oriented to reduce chain entanglements when the cellulose concentration was above 14 wt%, which led to a reduced relaxation time of the cellulose chains. From steady shear measurements, it was surprising to find that the viscosity versus shear rate curves exhibited four flow regions when the cellulose concentration exceeded 9 wt%, and meanwhile the Cox−Merz rule failed, which could be explained by the destruction of strong intra- and intermolecular hydrogen bonds between cellulose and the ionic liquid under shear deformation. The variation of the zero-shear viscosity, $\eta_0$, with cellulose concentration was consistent with the optical microscope observations. It was found that only positive $N_1$ values were observed over the entire shear rate range for all the studied solutions at 25 °C; nevertheless, a relatively positive minimum of $N_1$ appeared when the cellulose concentration exceeded 14 wt%. The $N_1$ values decreased with increasing temperature, and negative $N_1$ eventually appeared at 70 °C for the 18 wt% MCC/AMIMCl solution. Above the respective $T_c$, the viscosity versus shear rate curves only exhibited two flow regions due to melting of the liquid crystal phases. In summary, the results reported here could aid cellulose fiber production with concentrated cellulose/ionic liquid solutions.

**Acknowledgment.** Z. G. Wang acknowledges financial support from the National Science Foundation of China (grant number 10590355) for the Key Project on Evolution of Structure and Morphology during Polymer Processing and the start-up fund from the University of Science and Technology of China. J. Zhang acknowledges financial support from the National Key Technology R&D Program of China (grant number 2006BAC02A10) and the National Science Foundation of China (grant number 50873111).

## References and Notes

(1) Cai, J.; Zhang, L. *Biomacromolecules* **2006**, *7* (1), 183–189.
(2) Canejo, J. P.; Borges, J. P.; Godinho, M. H.; Brogueira, P.; Teixeira, P. I. C.; Terentjev, E. M. *Adv. Mater.* **2008**, *20* (24), 4821–4825.
(3) Lue, A.; Zhang, L. *J. Phys. Chem. B* **2008**, *112* (15), 4488–4495.
(4) Kosan, B.; Michels, C.; Meister, F. *Cellulose* **2008**, *15* (1), 59–66.
(5) Kuang, Q. L.; Zhang, J.; Wang, Z. G. *J. Phys. Chem. B* **2007**, *111* (33), 9858–9863.
(6) Zhang, H.; Wang, Z. G.; Zhang, Z. N.; Wu, J.; Zhang, J.; He, H. S. *Adv. Mater.* **2007**, *19* (5), 698–704.
(7) Remsing, R. C.; Hernandez, G.; Swatloski, R. P.; Massefski, W. W.; Rogers, R. D.; Moyna, G. *J. Phys. Chem. B* **2008**, *112* (35), 11071–11078.
(8) Xie, H. B.; Zhang, S. B.; Li, S. H. *Green Chem.* **2006**, *8* (7), 630–633.
(9) Fukaya, Y.; Sugimoto, A.; Ohno, H. *Biomacromolecules* **2006**, *7* (12), 3295–3297.
(10) Cao, Y.; Wu, J.; Meng, T.; Zhang, J.; He, J. S.; Li, H. Q.; Zhang, Y. *Carbohydr. Polym.* **2007**, *69* (4), 665–672.
(11) Xie, H.; King, A.; Kilpelainen, I.; Granstrom, M.; Argyropoulos, D. S. *Biomacromolecules* **2007**, *8* (12), 3740–3748.
(12) Granstrom, M.; Kavakka, J.; King, A.; Majoinen, J.; Makela, V.; Helaja, J.; Hietala, S.; Virtanen, T.; Maunu, S. L.; Argyropoulos, D. S.; Kilpelainen, I. *Cellulose* **2008**, *15* (3), 481–488.
(13) Wu, J.; Zhang, J.; Zhang, H.; He, J. S.; Ren, Q.; Guo, M. *Biomacromolecules* **2004**, *5*, 266–268.
(14) Zhao, H.; Jones, C. I. L.; Baker, G. A.; Xia, S.; Olubajo, O.; Person, V. N. *J. Biotechnol.* **2009**, *139* (1), 47–54.
(15) Cao, Y.; Wu, J.; Zhang, J.; Li, H. Q.; Zhang, Y.; He, J. S. *Chem. Eng. J.* **2009**, *147* (1), 13–21.
(16) Gericke, M.; Schlufter, K.; Liebert, T.; Heinze, T.; Budtova, T. *Biomacromolecules* **2009**, *10* (5), 1188–1194.
(17) Collyer, A. A. *Mater. Sci. Technol.* **1989**, *5* (4), 309–322.
(18) Postema, A. R.; Liou, K.; Wudl, F.; Smith, P. *Macromolecules* **1990**, *23* (6), 1842–1845.
(19) Boerstoel, H.; Maatman, H.; Westerink, J. B.; Koenders, B. M. *Polymer* **2001**, *42*, 7371–7379.
(20) Tseng, S. L.; Valente, A.; Gray, D. G. *Macromolecules* **1981**, *14* (3), 715–719.
(21) Werbowyj, R. S.; Gray, D. G. *Macromolecules* **1980**, *13* (1), 69–73.
(22) Swatloski, R. P.; Spear, S. K.; Holbrey, J. D.; Rogers, R. D. *J. Am. Chem. Soc.* **2002**, *124* (18), 4974–4975.
(23) Zhang, H.; Wu, J.; Zhang, J.; He, J. S. *Macromolecules* **2005**, *38* (20), 8272–8277.
(24) Zhou, M.; Han, C. D. *Macromolecules* **2006**, *39* (1), 232–242.
(25) Pearson, D.; Herbolzheimer, E.; Grizzuti, N.; Marrucci, G. *J. Polym. Sci., Part B: Polym. Phys.* **1991**, *29* (13), 1589–1597.
(26) Oertel, R.; Kulicke, W. M. *Rheol. Acta* **1991**, *30* (2), 140–150.
(27) Iizuka, E. *Mol. Cryst. Liq. Cryst.* **1974**, *25* (3−4), 287–298.
(28) Lin, Y. G.; Zhou, R.; Chien, J. C. W.; Winter, H. H. *Macromolecules* **1988**, *21* (7), 2014–2018.
(29) Kiss, G.; Porter, R. S. *J. Polym. Sci., Part C: Polym. Symp.* **1978**, 193–211.
(30) Kiss, G.; Porter, R. S. *J. Polym. Sci., Part B: Polym. Phys.* **1980**, *18*, 361–388.
(31) Kim, S. S.; Han, C. D. *J. Rheol.* **1993**, *37* (5), 847–866.
(32) Baek, S. G.; Magda, J. J.; Larson, R. G.; Hudson, S. D. In *Rheological Differences among Liquid-Crystalline Polymers. 2. Disappearance of Negative N(1) in Densely Packed Lyotropes and Thermotropes*; Boston Symposium on Liquid Crystals, Boston, MA, Oct, 1993; American Institute of Physics: Boston, MA, 1993; pp 1473−1503.
(33) Guo, J. X.; Gray, D. G. *Macromolecules* **1989**, *22* (5), 2082–2086.
(34) Kim, S. S.; Han, C. D. *Macromolecules* **1993**, *26* (24), 6633–6642.
(35) Grizzuti, N.; Cavella, S.; Cicarelli, P. *J. Rheol.* **1990**, *34* (8), 1293–1310.
(36) Doi, M. *J. Polym. Sci., Part B: Polym. Phys.* **1981**, *19* (2), 229–243.
(37) Leslie, F. M. *Arch. Ration. Mechan. Anal.* **1968**, *28* (4), 265-&.
(38) Marrucci, G.; Maffettone, P. L. *J. Rheol.* **1990**, *34* (8), 1217–1230.
(39) Marrucci, G.; Maffettone, P. L. *J. Rheol.* **1990**, *34* (8), 1231–1244.
(40) Larson, R. G. *Macromolecules* **1990**, *23* (17), 3983–3992.
(41) Kuang, Q. L.; Zhao, J. C.; Niu, Y. H.; Zhang, J.; Wang, Z. G. *J. Phys. Chem. B* **2008**, *112* (33), 10234–10240.
(42) Aharoni, S. M. *Macromolecules* **1979**, *12* (1), 94–103.
(43) Zakharova, S. S.; Jesse, W.; Backendorf, C.; van der Maarel, J. R. C. *Biophys. J.* **2002**, *83*, 1119–1129.
(44) Dong, Y. M.; Mao, W.; Wang, H. W.; Zhao, Y. Q.; Li, X. J.; Bi, D. X.; Yang, L. L.; Ge, Q.; Fang, X. M. *Polym. Int.* **2006**, *55*, 1444–1449.
(45) Chronakis, L. S.; Ramzi, M. *Biomacromolecules* **2002**, *3* (4), 793–804.
(46) Montembault, A.; Viton, C.; Domard, A. *Biomaterials* **2005**, *26* (14), 1633–1643.
(47) Morris, E. R. *Carbohydr. Polym.* **1990**, *13* (1), 85–96.
(48) Grizzuti, N.; Moldenaers, P.; Mortier, M.; Mewis, J. *Rheol. Acta* **1993**, *32* (3), 218–226.
(49) Guskey, S. M.; Winter, H. H. *J. Rheol.* **1991**, *35* (6), 1191–1207.
(50) Baek, S. G.; Magda, J. J.; Cementwala, S. *J. Rheol.* **1993**, *37* (5), 935–945.
(51) Baek, S. G.; Magda, J. J.; Larson, R. G. *J. Rheol.* **1993**, *37* (6), 1201–1224.
(52) Magda, J. J.; Baek, S. G.; Devries, K. L.; Larson, R. G. *Macromolecules* **1991**, *24*, 4460–4468.
(53) Kondo, T.; Togawa, E.; Brown, R. M. *Biomacromolecules* **2001**, *2* (4), 1324–1330.
(54) Aharoni, S. M. *Polymer* **1981**, *22* (3), 418–419.
(55) Kulicke, W. M.; Porter, R. S. *Rheol. Acta* **1980**, *19* (5), 601–605.
(56) Wan, Z. Z.; Li, L.; Cui, S. X. *Biopolymers* **2008**, *89* (12), 1170–1173.
(57) Hongladarom, K.; Burghardt, W. R.; Baek, S. G.; Cementwala, S.; Magda, J. J. *Macromolecules* **1993**, *26* (4), 772–784.
(58) Huang, C. M.; Magda, J. J.; Larson, R. G. *J. Rheol.* **1999**, *43* (1), 31–50.
(59) Aden, M. A.; Bianchi, E.; Ciferri, A.; Conio, G.; Tealdi, A. *Macromolecules* **1984**, *17* (10), 2010–2015.

JP1013863